Microstructural, mechanical and fracture characterization of lightweight microparticulate-reinforced multilayered metal matrix composite manufactured by accumulative roll bonding

Pereira G.S.1, Da Silva E.P.2, Requena, G.C3. Avila, J.A.4, Tarpani J.R.1,*

1. Department of Materials Engineering, University of Sao Paulo (USP), Av. Joao Dagnone 1100, Jd. Sta Angelina, 13563-120, Sao Carlos, SP, Brazil.
2. Institute of Engineering, Science and Technology (IECT), Federal University of Vales do Jequitinhonha e Mucuri (UFVJM), 39447-790, Janauba, MG, Brazil.
3. Institute of Materials Research German Aerospace Centre, Cologne, Germany.
4. Sao Paulo State University (UNESP), Campus of Sao Joao da Boa Vista, Av. Prof. Isette Correa Fontao, 505, Jardim das Flores, 13876-750, Sao Joao da Boa Vista, SP, Brazil.

*Corresponding author: jrpan@sc.usp.br

Research objective

To incorporate micro-silicon carbide particles (5 wt%) in commercially pure aluminum 1100 by accumulative roll bonding process and study microstructural changes and their effect on the mechanical properties and fracture mechanisms.

Research goals

- Manufacture micro-silicon carbide particles-reinforced metal matrix composite laminate via accumulative roll bonding by adopting affordable fabrication route.
- Microstructural characterization by scanning electron microscopy, energy dispersive X-ray spectroscopy, computed X-ray microtomography, backscattered electron diffraction and X-ray diffraction to determine potentially acting strengthening mechanisms.
- Mechanical characterization by hardness, notch tensile and ball-cratering wear tests to envision potential application field for the end-product.

- Fracture inspection to identify and characterize operating failure mechanisms as affected by the reinforcing particulate phase.

Highlights

Accumulative roll bonding process after 7 lamination passes reasonably dispersed micro-scale reinforcing particles in aluminum matrix.

1. Silicon carbide particles imparted hardness and only moderately enhanced tensile properties of unnotched and notched specimens.
2. The metal matrix laminate was insensitive to geometrical stress raisers in terms of ultimate strength, stiffness and toughness at maximum load.
3. The ceramic particulate granted outstanding wear resistance to the composite laminate by acting as effective solid lubricant.
4. Shear and dimple nucleation, growth and coalescence fracture mechanisms prevailed in tensile loading, while abrasion, adhesive and lamination mechanisms governed wear properties

ABSTRACT: Accumulative roll bonding is a severe plastic forming process recently proposed to manufacture ceramic particle reinforced-multilayered metal matrix composites. In this work, 5 wt% micro-scale silicon carbide particle-reinforced commercially pure aluminum 1100 composite laminate was produced through roll bonding. Microstructural features, hardness, tensile properties in the presence of stress concentrators, and wear resistance were assessed. Fracture surface inspection was carried out to determine operating failure mechanisms. Hardness and tensile properties were not substantially improved by ceramic particles incorporation. Main reasons for this behavior were limited grain refinement and strain-hardening due to periodic annealing at relatively low temperature, only moderate spatial dispersion of particulate phase, particle agglomeration and mild porosity content due to relatively large particle size. Though tensile properties increments were not so attractive, exceptional increase in wear performance was achieved due to the addition of ceramic particulate phase, which acted as solid lubricant mitigating to a large extent adhesion, abrasion and lamination wear mechanisms.

Keywords: Accumulative roll bonding; fracture mechanisms; mechanical properties; notch effect; particulate reinforced-metal matrix composite.

1. Introduction

Ceramic particulate reinforcing-metal matrix composites (hereafter MMC) offer higher specific elastic modulus and ultimate strength (properties/weight ratios), better corrosion and wear resistance and greater thermal and dimensional stabilities than the base metal [1,2]. However, the expanded use of this composite material has been limited by its high manufacturing costs according to the routes currently available, such as powder metallurgy, casting, spray casting and positive and negative (vacuum) pressure infiltration. On the other hand, traditional technologies like strip and ingot casting followed by secondary mechanical processes present poor reinforcing-particles dispersion, high porosity levels and weak bonding between ceramic reinforcement and metal matrix leading to deficient mechanical properties [2,3,5].

To overcome these constraints, accumulative roll bonding (hereafter ARB) process, a genuinely continuous solid-state manufacturing route used to increase the mechanical performance of metal sheets via grain size refinement and strain-hardening mechanisms [6,7], has been proposed for obtaining low-cost, continuous large-scale production, increased strength and structurally refined multilayered microparticulate-reinforced MMC composites [5]. Strictly speaking, ARB is a method of rolling a stack of metal sheets, which are repeatedly rolled to a severe reduction ratio under harsh shear and compressive loads, sectioned into two halves, piled again to be the initial dimension and rolled. Typically, less than 12 rolling passes have been employed by researchers to manufacturing SiCp-reinforcing MMC via ARB. This technique can be easily adapted and integrated into existing continuous industrial rolling trains without major modifications and be scaled up to produce low-cost laminated materials with an ultra-fine-grained microstructure [8]. ARB is not only a heavy-straining process but also a solid-state deformation bonding method, and large strains can be accumulated in the metallic laminate without any geometrical change in the worked piece. Redundant shear

strain due to large friction during rolling can lead to ever-increasing through-the-thickness microstructure refinement and uniformity [9-11].

Improved SiCp dispersion, low porosity, imparted tensile and layer bond strengths have been reported in ARB-processed MMC comprising particulate silicon carbide (hereinafter SiCp) reinforcing commercially pure aluminum (henceforth Al) from 1050 to 1100 grades [4,5,12]. Lower initial thickness, higher rolling speed and large rolling reduction have been determined as essential factors for improving bond strength. The effect of pre-, post- and continuous rolling annealing on SiCp scattering, metal formability related to work-hardening recovery, recrystallization, interlayer diffusion and consolidation (bond strength) has also been investigated [13-16].

Lee et al. [17] found that variations in the ultimate tensile strength of Al-1100 base metal and the corresponding MMC with 5 vol% SiCp simultaneously submitted to the ARB process was similar. However, due to higher matrix grain refinement in the MMC as a result of the presence of the ceramic particulate, the strength gain of the Al-SiCp composite was larger than the base metal. The same trend regarding grain refinement acceleration and efficacy due to ceramic particulate presence was observed by Alizadeh et al. [18] working with Al-1100 7 vol% SiCp composite.

Regarding the reinforcing particle size effect, Jamaati et al. [19] cold worked Al-1050 with vol% 10 SiCp and discovered that microstructural refinement evolution, reinforcing particle dispersion and low porosity tensile strength with larger (40 μm) particles was more remarkable and earlier attained than 2 μm particle size.

Wagih et al. [20] investigated ARB to produce Al-1050 4 vol% SiCp composite and determined the main strengthening mechanisms as grain refinement, strain-hardening due to rolling process, while the addition of SiC nanoparticles acts as a secondary strengthening source.

Melaibari et al. [21] studied ARB to manufacture Al-1050 5 vol% SiC composite and observed that warm accumulative roll bonding breaks reinforcing particles agglomerates thus improving their uniform dispersion throughout the metal matrix, and so hardness, strength, ductility, toughness and bond strength were imparted.

Fathy et al. [22] evaluated the mechanical properties of MMC comprising Al-1050 base metal and 1 to 4 vol% reinforcing SiCp and emphasized the strong mechanical bonding taking place at the interface of the particle matrix, thus improving hardness, tensile

strength and elongation, and determined the fracture mechanism was by shear ductile rupture.

Darmiani et al. [23] researched the wear resistance of Al-1050 containing 4 wt% nanometric SiC particles and accredited the improved performance to increasing uniformity of ceramic particle distribution in the metal matrix, grain refinement and strain-hardening effects achieved during ARB cycles.

Potential strengthening mechanisms in SiCp-reinforced Al matrix ARB composites been summarized, namely, grain size refinement and well-developed high-angle grain boundaries causing dislocation pile-up, strain-hardening on the metal matrix, elastic and thermal mismatches, Orowan effect, back stress strengthening and work-hardening at the SiCp-Al boundary, besides load-transfer to the particulate phase. The operation, or not, of one or more mechanism in a determined MMC laminate depends upon the lamination processing parameters, the average particle size, particle size and dispersion, metal-ceramic interaction, detrimental phases and porosity formation [13,24].

In the present work, an investigation is carried out regarding microstructural, mechanical and fractographical characterization of MMC comprising micro-SiCp dispersed in commercially pure Al-1100 by economical ARB route. The multilayered MMC had as reference both the as-received Al-based foil and corresponding as-roll bonded laminate. Easily and rapidly fabricated, low-cost, notch insensitive MMC laminate, which can be employed in low-demanding applications where stringent wear performance is required, has been obtained.

2. Materials

Commercially pure Al-1100 grade (chemical composition in Table 1) received as 0.4 mm-thick cold-rolled strips was utilized as the base-metal material. It typically exhibits good mechanical formability, excellent corrosion resistance, low cost and wide availability. The as-received Al-1100 lamina was annealed at 350°C in N2 atmosphere for 2 h to enhance their mechanical workability for subsequent ARB process.

Large average size (25 μm) low-cost commercial SiCp were employed as reinforcing phase due to their well-balanced properties, such as low density, high hardness and wear resistance, high thermal conductivity and thermal shock resistance and broad availability.

SiCp were heat-treated at 900ºC in air atmosphere for 2 h for surface decontamination and SiO2 coating formation to improve compatibility and interaction with the metal matrix phase [4,5,13,22].

Table 1. Chemical composition (wt%) of Al-1100 base metal.

Al	Si	Mn	Cu	Others
Balance	0.94	0.05	0.01	0.05

3. Experimental procedures

3.1 **MMC m**anufacture

Four annealed Al-1100 strips with in-plane dimensions of 200 x 50 mm^2 were cleaned with organic solvent and brushed with steel bristles to remove the surface oxide layer and create roughness texture to induce metal/metal and metal/ceramic interaction. 2.5 wt% of SiCp were then uniformly dispersed in appropriate amount onto the surface of three Al-1100 strips, which were then clamped by a steel wire along with the covering fourth strip to prevent their relative movement during the rolling process. Rolling direction was the same as the as-received Al-1100 strip.

Mechanical working progressed without lubrication in a double cold cylinder rolling mill with 13 tons radial load-capacity and rolls with diameter of 100 mm, whose speed was fixed at approximately 50 mm/min. A thickness reduction of 37.5% was imposed in the first lamination pass and 50% in the next six ones, for a total of just 7 passes, and the final laminate thickness was 1 mm. After each rolling cycle, the worked piece was cut in half and the two halves stacked together for a consecutive pass. SiCp were still added in the second and third cycles (1.25 wt% per cycle) to obtain the targeted 5 wt% SiCp-MMC laminate. The samples were heated in oven at 345ºC for only 10 minutes before each

rolling pass aiming at recovering work-hardening introduced in previous cold rolling cycle to enhance formability.

Identical procedures as above, except for SiCp addition, were applied to four annealed Al-1100 strips, and the strengthening role played by SiCp in the multilayered MMC could therefore be identified.

To determine the effects of ARB process per se, the as-received 0.4-mm thick Al-1100 strip was also mechanically and fractographically characterized.

All tensile tests were performed with the axial loading applied in the lamination direction.

Table 2 lists the variables of the ARB manufacturing process.

Table 2. ARB process variables.

Number of passes	Process temperature (°C)	Number of Al-1000 layers	Initial thickness of MMC per pass (mm)	Final thickness of MMC per pass (mm)	Thickness reduction per pass (%)
1	345	4	1.6	1	37.5
2	345	8	2	1	50
3	345	16	2	1	50
4	345	32	2	1	50
5	345	64	2	1	50
6	345	128	2	1	50
7	345	256	2	1	50

3.2 Microstructural analysis

Spatial SiCp distribution in the multilayered MMC, consolidation levels and porosity profiles of both ARB products were evaluated by scanning electron microscopy (SEM)

in FEI™ model Inspect F-50 operating in both secondary (SE) and backscattered (BSE) electron modes. It was equipped with Link Analytical™ Isis system for quali and quantitative elemental analysis (EDX). Computed X-ray microtomographer (mCT-XR) RayScan™ model 250E complemented the SEM analysis.

Zeiss™ model Ultra 55 electron backscattering diffraction (EBDS) microscope and Panalytical™ X Pert PRO X-ray diffraction (XRD) equipment were utilized to identify possible phases transformation caused by ARB process, besides recrystallization, strain-hardening mechanisms and crystallographic texture.

Samples preparation avoided deformation and the presence of oxides layers on the inspected surfaces. Manual wet grinding till 4000 mesh sandpaper and automated polishing with colloidal silica following 0.25 μm diamond paste were employed.

3.3 Mechanical properties

Zwick-Roell™ ZHVμ micro Vickers hardness tester was used to determine potential strengthening mechanisms operating during ARB process per se, and due to SiCp incorporation. Five measurements were performed in each sample, and average and standard-deviation values were obtained.

Monotonic tensile tests were carried out with cold-rolled Al-1100 foil (baseline condition), Al-1100 and Al-SiCp MMC ARB laminates. Small-scale full-thickness specimens with length and width of, respectively, 120 and 12.7 mm were tested according to the ASTM E8M standard. Unnotched and notched test pieces, presented in Fig.1, were studied. Tests were conducted at room temperature in specimens with the longitudinal axis parallel to the rolling direction; EMIC™ universal tensile test machine equipped with 5 kN load-capacity cell and operating under displacement control at strain rate of 2 mm/min was used. Strain was monitored throughout the test by an extensometer with initial gouge length of 25 mm. Tests were repeated three times for each material and specimen conditions up to complete rupture of the test coupons. Engineering stress-strain curves (load divided by gross section of the specimen) were plotted and average and standard-deviation values of typical mechanical properties like ultimate tensile strength and ductility (strain at fracture) were determined.

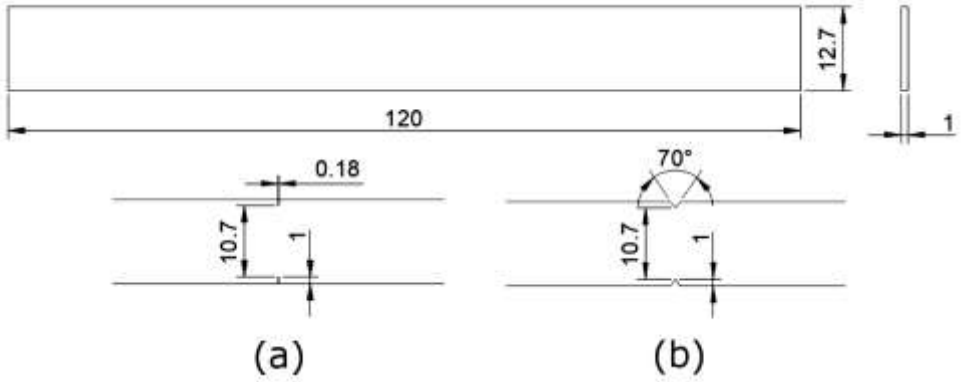

Figure 1. Notch geometries and dimensions in tensile test specimens: (a) slit (curvature radius of 0.075 mm), (b) V-notch (0.125 mm).

Ball-cratering wear tests were performed under dry conditions (micro-adhesion wear was privileged) on fixed sphere equipment. SAE 52100 steel sphere with 25.4 mm in diameter travelling at 300 rpm and contacting the sample under 0.66 N load was utilized. Samples surface preparation included progressively grinding till 2000 mesh sandpaper and cleaning in ultrasonic bath with acetone after each step. At the traveled distances of, respectively, 120, 239, 478 and 957 m (i.e., time travels 5, 10, 20 and 40 min) the spherical worn calottes were cleaned and photographed with Carl Zeiss™ model Axio Lab.A1 optical microscope for subsequent diameter measurement and removed volume calculation [25].

FEI-SEM™ model XL50 operating in secondary electron mode was used to characterize the morphological aspects of worn surfaces.

4. Results and discussion

4.1 Microstructural analysis

4.1.1 Scanning electron microscopy (SEM)

Figure 2 shows SEM images of cross-sectioned Al-1100 strip and Al-1100 MMC ARB laminates. Figure 2(a) shows practically inclusion-free Al-1100 ARB laminate, while Fig.

2(b) reveals the presence of few small pores. The homogeneous texture of the laminate is confirmed, since the interfaces of the multilayered structure cannot be easily identified even under high magnification. Figures 2(c-e) refer to the Al-SiCp MMC laminate after four accumulated rolling steps, where a relatively poor SiCp dispersion is noticed in Fig.2(c) as aligned ceramic particulate aggregation mainly located at the multilayer interfaces. Figure 2(d) presents a large pore created when a SiCp agglomerate was pulled out during the metallographic preparation. Fig.2(e) displays a large SiC particle, along with smaller ones surrounded by the ductile matrix, indicating proper physical interaction between the phases. However, an intermediate size particle at the bottom of the figure does not exhibit that desirable feature.

Figures 2(f-h) refers to the multilayered MMC laminate after seven ARB passes, i.e., end-product. Segmented lines of agglomerated SiCp are noticed in Fig.2(f), indicating increased, though still moderate SiCp homogenization in the metal matrix due to additional lamination passes. Figure 2(g) presents much smaller defects than observed in Fig.2(d), thus confirming less critical SiCp agglomerates in the latter case. SiC particle breakage and debonding can be observed in Fig.2(h).

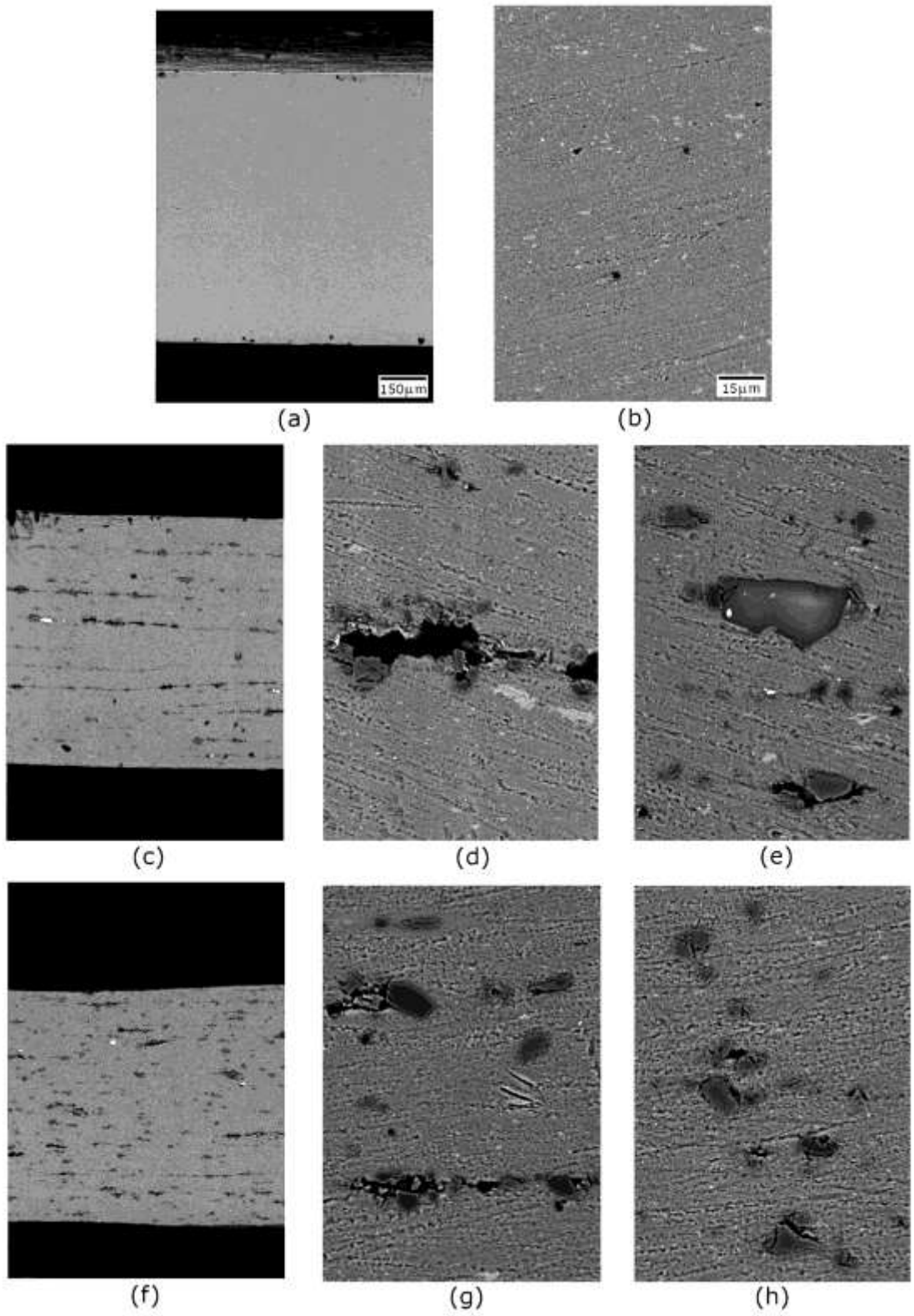

Figure 2. (a) Low and (b) high magnification SEM images (SE mode) of Al-1100 ARB laminate; (c,d,e) general and magnified views of MMC laminate after four rolling passes and (f,g,h) after seven rolling passes (BSE mode). Laminate thickness corresponds to the

page height and lamination direction to the page width. Images (a), (c) and (f) taken at the same magnification. The same is true for the remaining images.

4.1.2 Energy dispersive X-ray spectroscopy (EDX)

Figure 3 shows EDX chemical maps of cross-sectioned MMC laminate (same views as Fig.2). Small amounts of iron and carbon evenly distributed through the MMC bulk resulted from contamination by lamination rollers. Fairly good local dispersion of SiC particles and presence of oxygen-formed inclusions are revealed. There is no indication of extraneous phases formed during the ARB process.

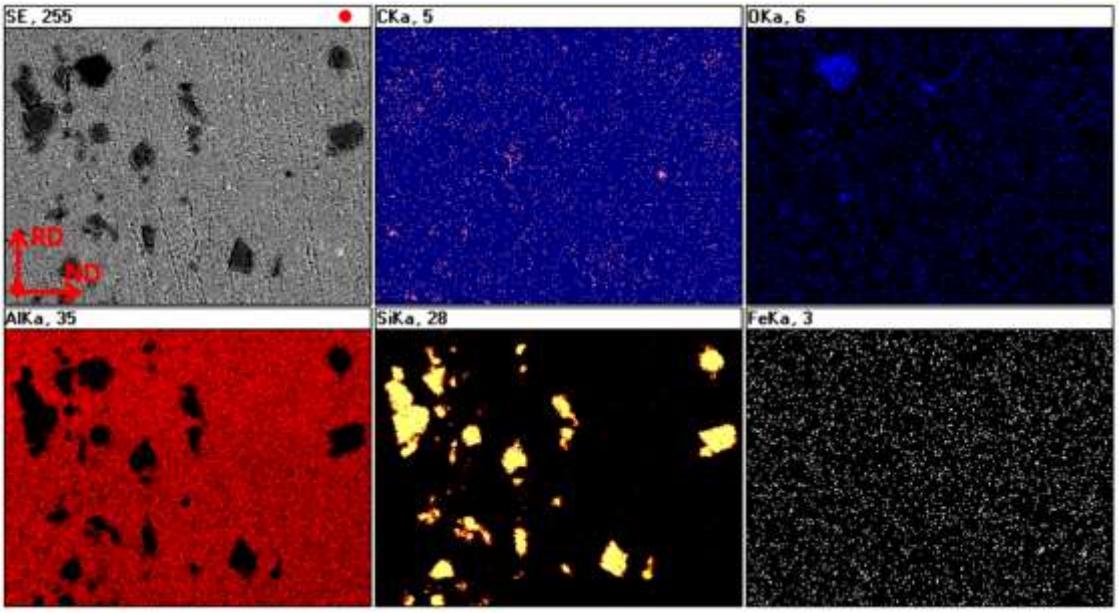

Figure 3. Chemical mapping of MMC laminate. MMC lamination direction corresponds to the page height and laminate width to the page width.

4.1.3 Computed X-ray microtomography (mCT-XR)

X-ray microtomographies of reinforcing SiCp phase are presented in Fig.4. Figure 4(a) refers to the spatial distribution map of high-density ceramic particles only, while Fig.4(b) shows all-densities SiCp dispersed in the MMC laminate. Though the 500 μm-thick

tomography slice is ten times thicker than the maximum SiC particle size, impoverished areas can still be detected in both images, so confirming previous images in Fig.2.

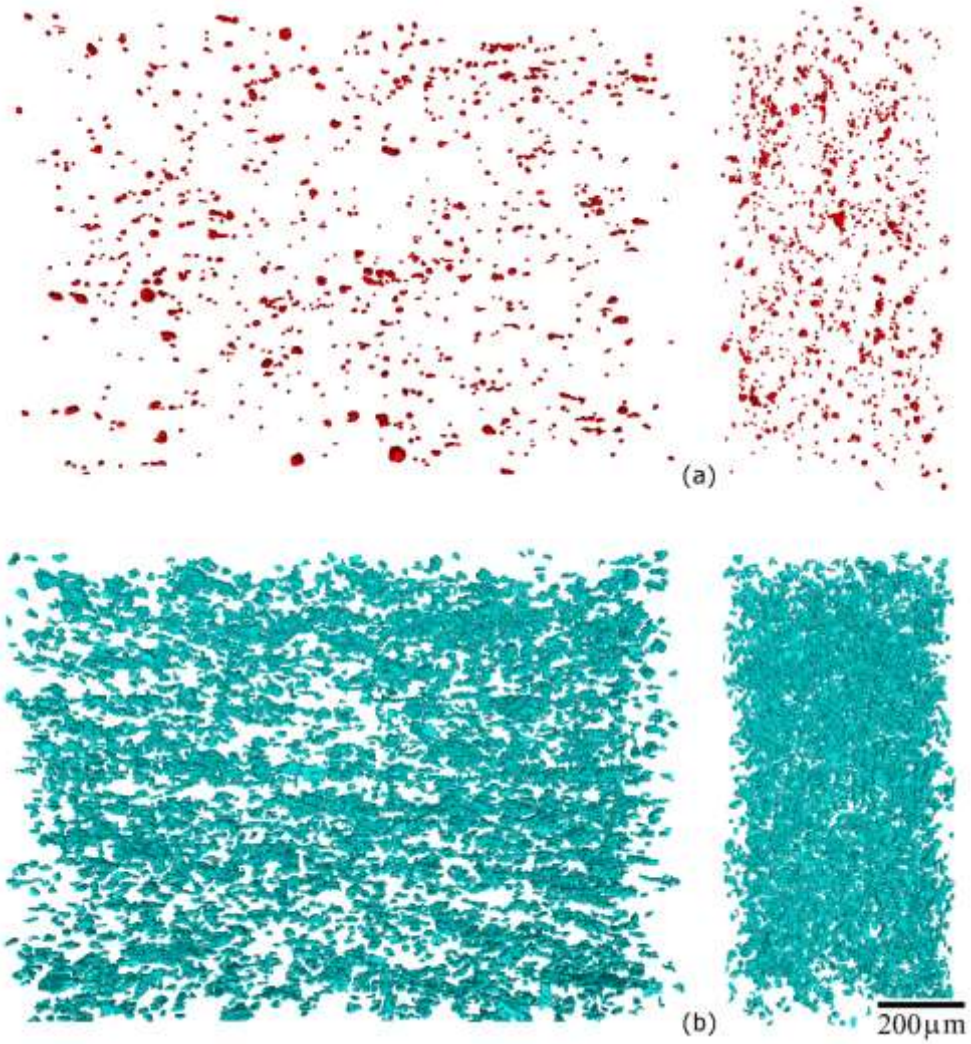

Figure 4. SiCp distribution maps from X-ray microtomography analysis: (a) highest density SiCp, (b) all-densities SiCp. At left, MMC lamination direction corresponds to the page width and thickness direction to the page height; at right, MMC laminate thickness direction corresponds to the page height and sample width to the page width.

4.1.4 Electron backscattering diffraction (EBDS)

Figure 5 shows the EBDS inverse pole figure of Al-1100 ARB laminate, where colors are indexed to specific crystal orientations. Interlayer bonding failure exhibits black staining indicating no crystallographic indexation.

Very deformed and elongated grains (high-angle boundaries) in the lamination direction are observed, with some subgrains (low-angle boundaries) within them. There are no evidences that recrystallization has occurred, implying that only limited work-hardening must have been developed in the last rolling pass and/or accumulated from previous passes to act as recrystallization driving force.

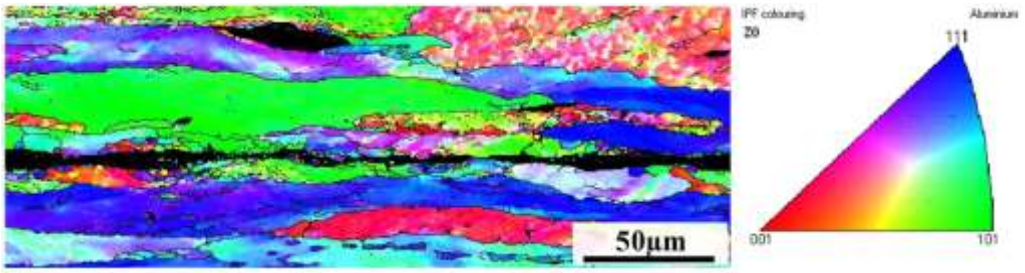

Figure 5. Inverse pole figure map of Al-1100 ARB laminate. Laminate thickness corresponds to the page height and lamination direction to the page width.

Figure 6 presents the inverse pole figure of MMC laminate, where only the Al phase was indexed in search for work-hardening and recrystallization evidences. Delaminations and SiC particles are black stained meaning no crystallographic indexation. Grains were less deformed than the Al-1100 ARB laminate (Fig.5). Previous researches [2,13,18] report that when the SiCp-reinforced MMC is exposed to severe plastic deformation, highly localized stress develops in the vicinity of ceramic non-deformable particles, which form barriers that inhibit the elongation of the metallic grain. According to the authors, this morphology modification may induce nucleation of substrate grains by introducing high dislocation density. This “particle stimulated recrystallization process” seems not have been effectively triggered in the present case, substantiating previous assumption that previous or accumulated work-hardening did not provide activation energy enough to recrystallization. In other words, pre-heating (345C° for 10 minutes) before each ARB cycle was much possibly effective in recovering metal formability [26-28]. The large average size of SiCp must have also affected this lack of recrystallization as well, which means absence of grain refinement [29-31].

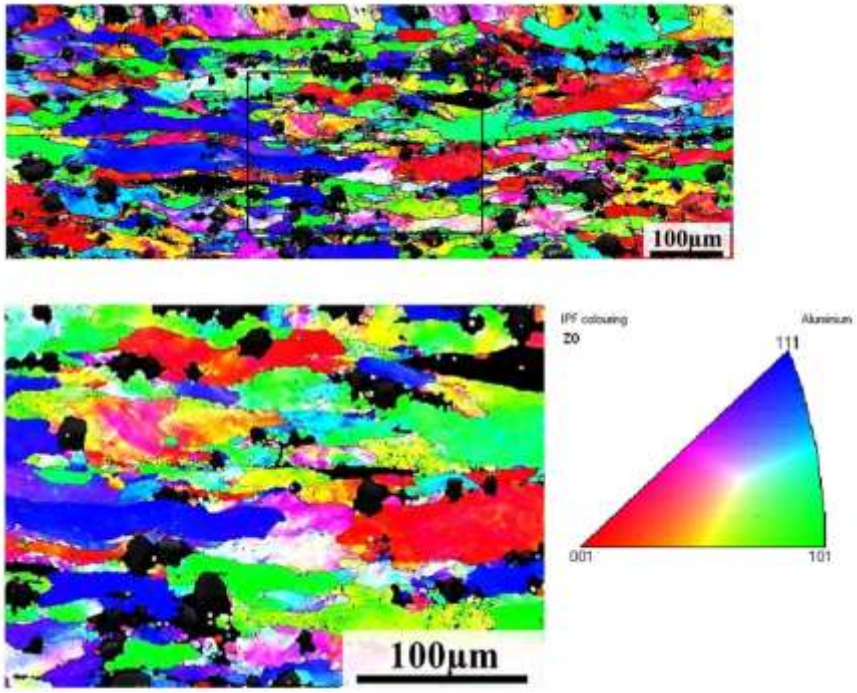

Figure 6. (a) Inverse pole figure map of the MMC laminate, (b) magnified view of black rectangle field. Laminate thickness corresponds to the page height and lamination direction to the page width.

Oliveira et al. [32] observed finely dispersed precipitates in as-received Al-1100 sheets preventing recrystallization by restraining sub-boundaries movement. Recrystallization only occurred above 400°C following cold rolling to 80% area reduction. This indicates that the same mechanism must also have contributed to inhibited recrystallization in the present study, since area reduction on rolling passes was 50%, and subsequent annealing was carried out at 345°C.

Figure 7(a) shows the same MMC microstructure as in Fig.6, where metal matrix and ceramic particles are portrayed in red and blue colors, respectively. One can observe only moderate distribution of SiC particles in the metal bulk, as well as their trend to align as agglomerates in the interlayer planes, as previously revealed by Fig.2. On the other hand, Fig.7(b) highlights tiny discrete recrystallized regions in blue, as originated by subgrain rotation [33], thus confirming past findings through inverse pole figure maps.

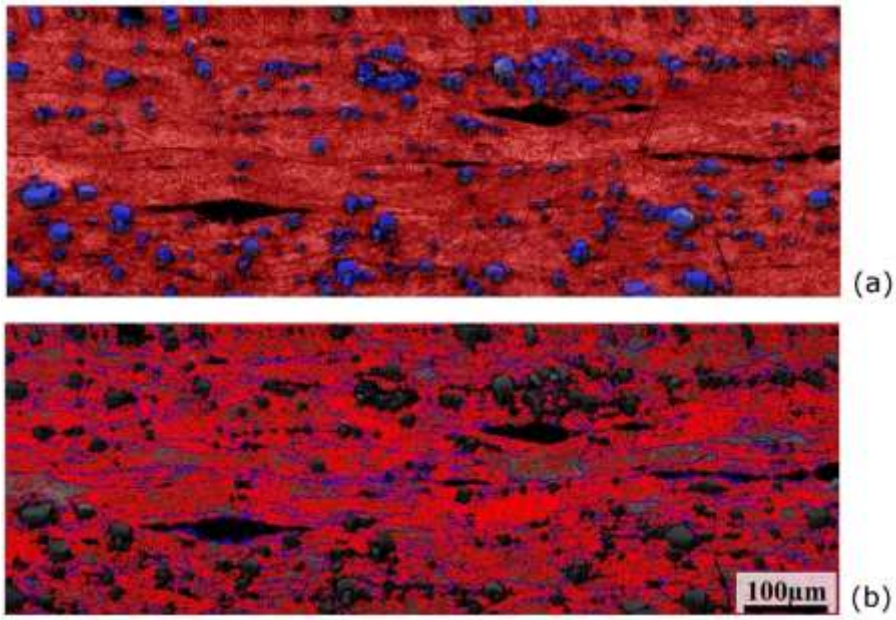

Figure 7. (a) MMC microstructure featuring metal matrix (red) and SiC particles (blue); (b) recrystallization map (highlighted in blue). Laminate thickness corresponds to the page height and lamination direction to the page width.

Quali and quantitative analyses of acting strengthening mechanisms in the matrix phase of the composite are presented in Fig.8. Figure 8(a) shows small and sparse recrystallized regions in blue color, whereas Fig.8(b) differentiates red colored high-angle pancaked grains boundaries, above 15º, from less deformed low-angle yellow subgrains, between 2-15º. In situ observation [34] indicates that low and particularly high-angle grain boundaries prevent dislocation glide across them, with the main sources of the impediment possessing geometrical and local structural stabilization natures.

Figure 8(c) illustrates areal frequency distribution histogram of the above described mechanisms, permitting one to infer their magnitude in strengthening the MMC laminate.

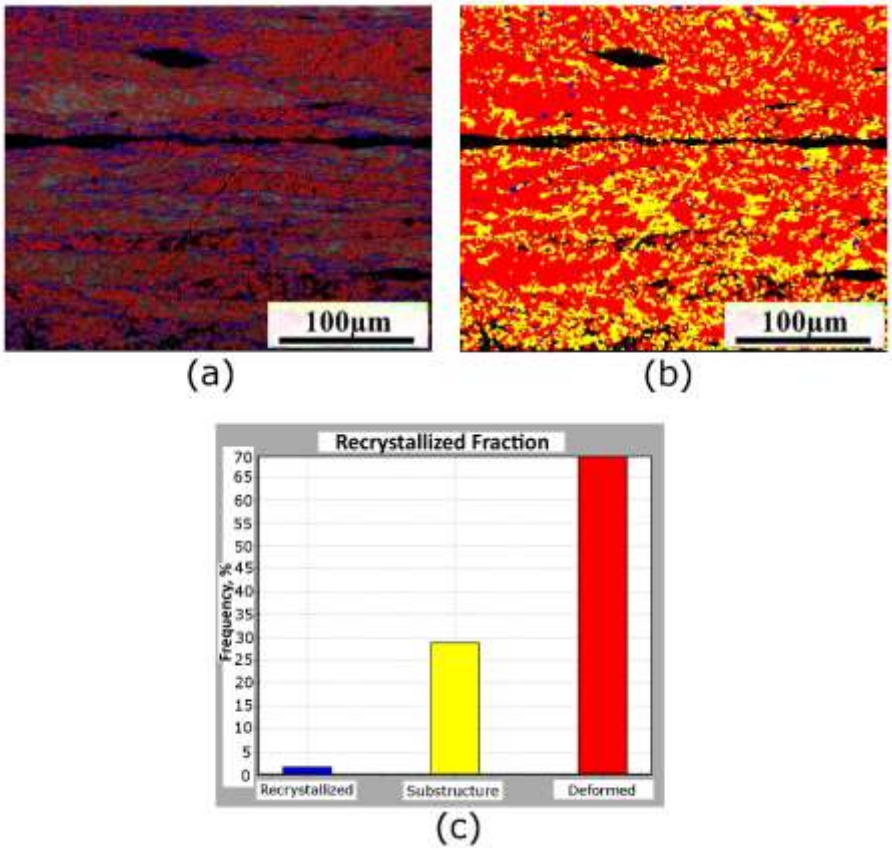

Figure 8. (a) Recrystallization, and (b) low and high-angle grain maps; (c) corresponding percentage area-based histogram. Laminate thickness matches the page height and lamination direction the page width.

Figure 9 shows stereographic projections for the Al-SiCp composite according to three different crystallographic orientations, as obtained by EBSD. The pole figures refer to the plate rolled surface.

Preferential crystallographic orientations of grains (rolling texture) with a maximum intensity of 3.57x is noticed. The strain-hardened structure in the lamination direction derives from plastic deformation according to preferential crystallographic slip planes. The highest intensity (3.57x) is observed for the densest CFC lattice plane family {100} (i.e., rotated cube texture), with deformation texture developing with the cube surface almost parallel to the plate surface, which is characteristic of cold rolling [35].

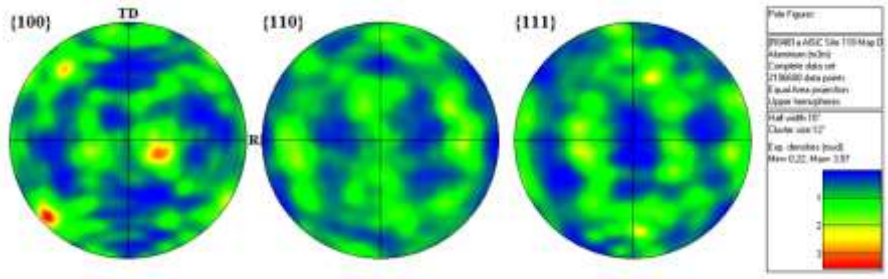

Figure 9. Stereographic projections for the Al-SiCp MMC. The rolling direction corresponds to the page width, and the plate width to page height.

4.1.5 X-ray diffraction (XRD)

Figure 10 shows X-ray diffractograms obtained for both Al-1100 ARB and Al-SiCp MMC samples. In the former case, only peaks belonging to Al-1100 are present, while peaks belonging to, respectively, Al-1100 and SiCp are revealed for the MMC laminate. Therefore, no extraneous phases have been generated during ARB manufacturing that could impair the end-products performance. These results agree with previously obtained via EDX analysis and emphasize the advantages of solid-state fabrication process over other techniques [2].

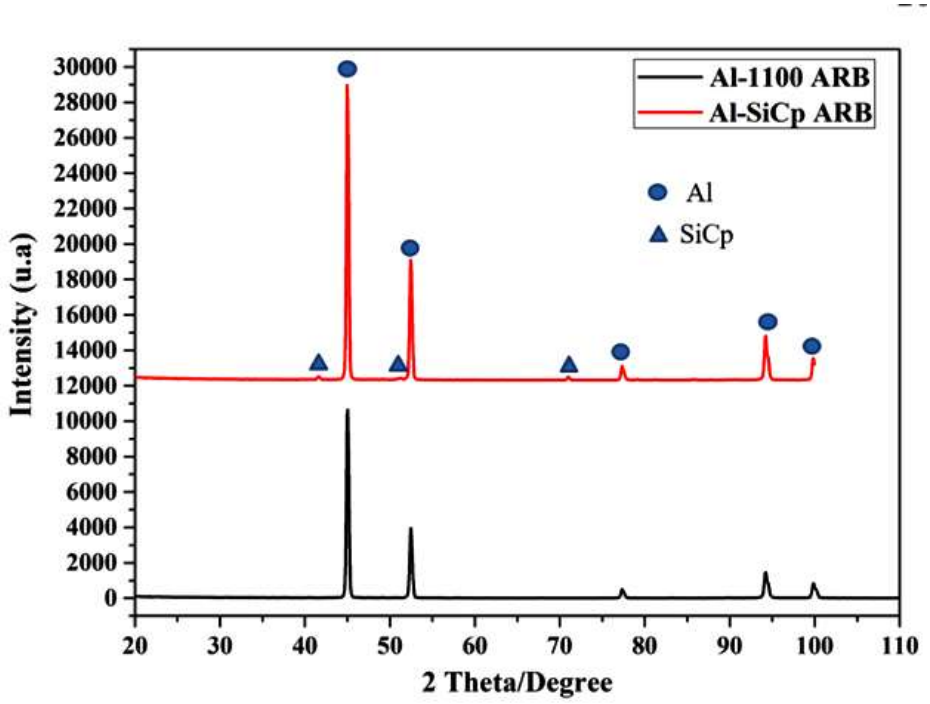

Figure 10. X-ray diffractograms of Al-1100 and Al-SiCp ARB laminates.

4.2 Mechanical properties

4.2.1 Vickers hardness

Table 3 provides five hardness measurements, average and standard-deviation values for both ARB end-products.

Table 3. Hardness testing results for the ARB end-products.

Al-1100 ARB	Al-SiCp MMC ARB
45.0	68.0
45.4	67.0
44.8	70.7
44.9	66.6
45.4	66.2
45.1 (0.3)	67.7 (1.3)

The ARB-laminate´s hardness is much lower than reported by Santos-Filho [26] for the same Al-1100 material after annealing at 200°C, which was circa 55 HV. According to those authors, grain refinement along with only partial work-hardening recovery during the heat treatment led to high hardness material. Considering that in the present work annealing was performed at substantially higher temperature (345 C°) and that recrystallization has practically not been developed in the end-product, hardness values can be considered consistent. Table 3 also confirms that the ARB-MMC laminate is significantly harder than ARB-laminate, as a result of SiCp incorporation.

4.2.2 Monotonic notch tensile testing

Average and standard-deviation values of ultimate tensile strength and strain at rupture are listed in Table 4. The engineering stress-strain curves for materials and specimen geometries tested are shown in Figs.11 and 12.

Table 4. Tensile testing results for all materials and specimen geometries tested.

Material	Ultimate tensile strength (MPa)		Strain at rupture (%)	
	Mean	SD	Mean	SD
Al-1100	119	2.7	2.3	0.3
Al-1100 ARB	122	2.6	5.5	0.4
Al-SiCp ARB	133	3.1	6.3	0.3
Al-1100 slit-notch	67	1.6	6.5	0.2
Al-1100 ARB- slit-notch	108	1.9	2.2	0.7
Al-SiCp ARB- slit-notch	128	1.9	1.5	0.1
Al-1100 V-notch	65	1.4	6.3	0.9
Al-1100 ARB- V-notch	119	1.8	3.3	0.2
Al-SiCp ARB- V-notch	126	1.7	1.8	0.1

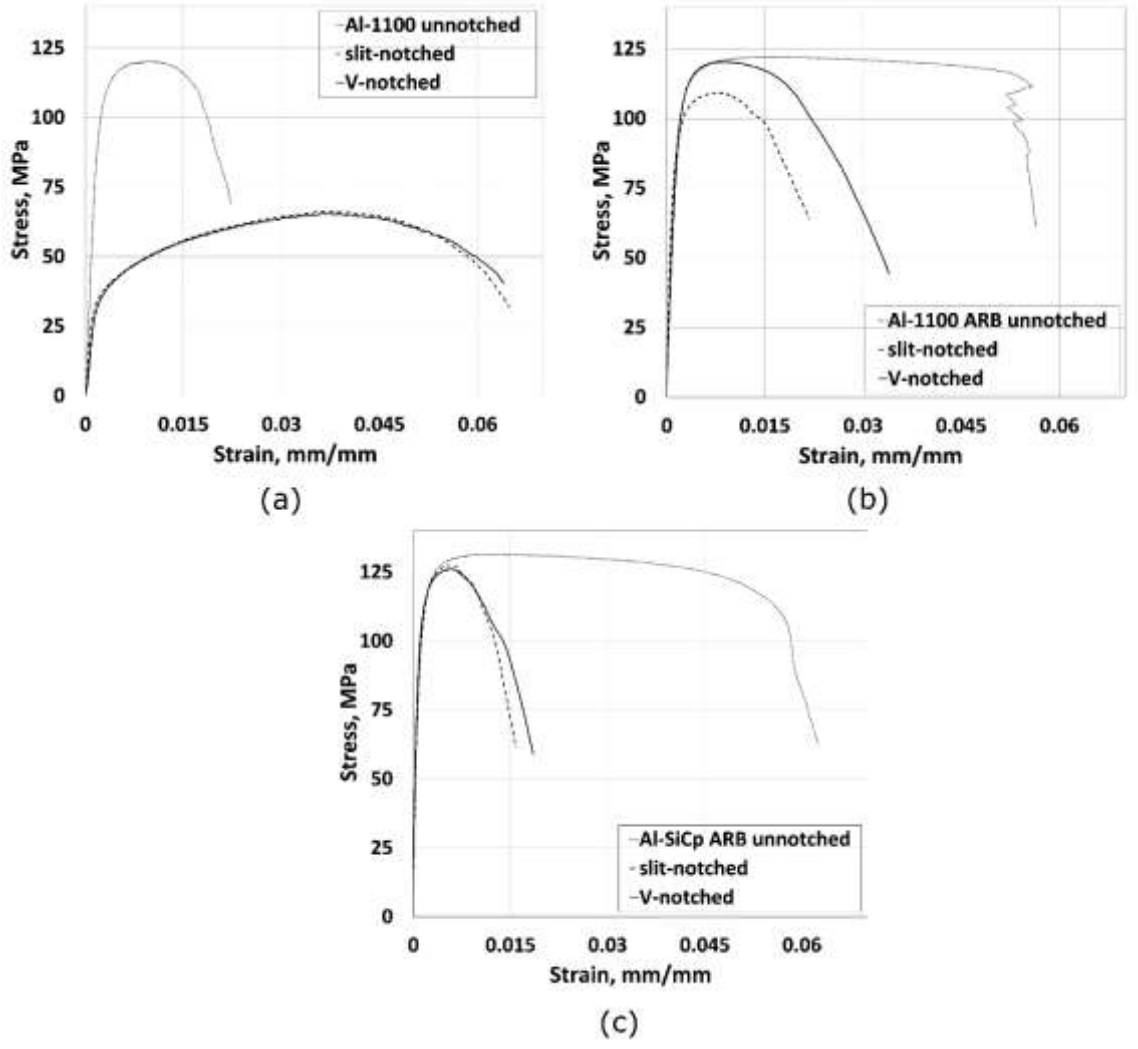

Figure 11. Engineering stress-strain curves for the three tested materials according to the specimen geometry.

The high ultimate strength of as-received unnotched Al-1100 strip in Fig.11(a) indicates that high degree of work-hardening was attained during cold-rolling [14,22,36,37]. Figure 11(b) shows that the Al-1100 ARB laminate approached well the as-received Al-1100 strip in terms of mechanical strength. Considering that the latter material was annealed before each of the 7 lamination passes, thus relieving previously imposed strain-hardening, other reinforcing mechanisms, typical of metal laminated structures must have operated. According to the literature [38-41], lamination processing induces extra strain-hardening at the contacting surfaces of two adjacent laminae (interface-affected-zone). In turn, back stress strengthening and back stress work-hardening operating at the strain-hardened interfaces confine dislocation motion within the layers, and powerful reinforcing mechanism are activated in the whole laminate. In fact, outstanding laminate toughening has also been reported [38-40] under such circumstances according the pre-delamination effect, whereby cracks nucleate in every formed interface-affected-zone, leading to high energy consumption during crack propagation caused by in-plane shear stresses. This toughening effect can be confirmed by comparing stress-strain curves of unnotched specimens in Figs.11(a-c), where exceptional ductility of ARB-products contrasts with the restricted elongation of the as-received Al-1100 sheet.

Figure 11(a) also shows that the Al-1100 lamina is highly notch-sensitive, and the material weakens in the presence of geometrical discontinuities. This behavior is caused by larger plastic zone ahead the notch tip, thus resulting in stress relaxation [42]. According to Fig.11(b), the Al-1100 ARB laminate is sensitive to the slit-notch geometry, which is sharper than V-notch, but still in a much less extent than the Al-1100 sheet. Differently from the as-received Al-1100 lamina, strain at fracture (ductility) decreases in the Al-1100 ARB laminate when stress concentrators are introduced. The multilayered nature of ARB structure facilitates delamination that absorbs energy at the expenses of plastic zone growth at the notch-tip (notch-induced embrittlement), granting the ARB laminate more fracture-prone.

The same mechanisms act as well in the notched Al-SiCp multilayered MMC laminate. However, due to the presence of fragile SiC particulate, brittle behavior is enhanced and the material becomes notch-insensitive at all in terms of ultimate strength, stiffness and

toughness till maximum load-carrying capacity. Since that intentional and non-intentional discontinuities are inevitable, and present a variety of geometries and root radii, the advantage of the manufactured MMC over its rivals is established.

Figure 12 essentially replots the same stress-strain data provided in Fig.11, nonetheless it allows better way to compare the mechanical performance of the materials tested. For instance, the MMC supremacy in all the tensile properties becomes evident.

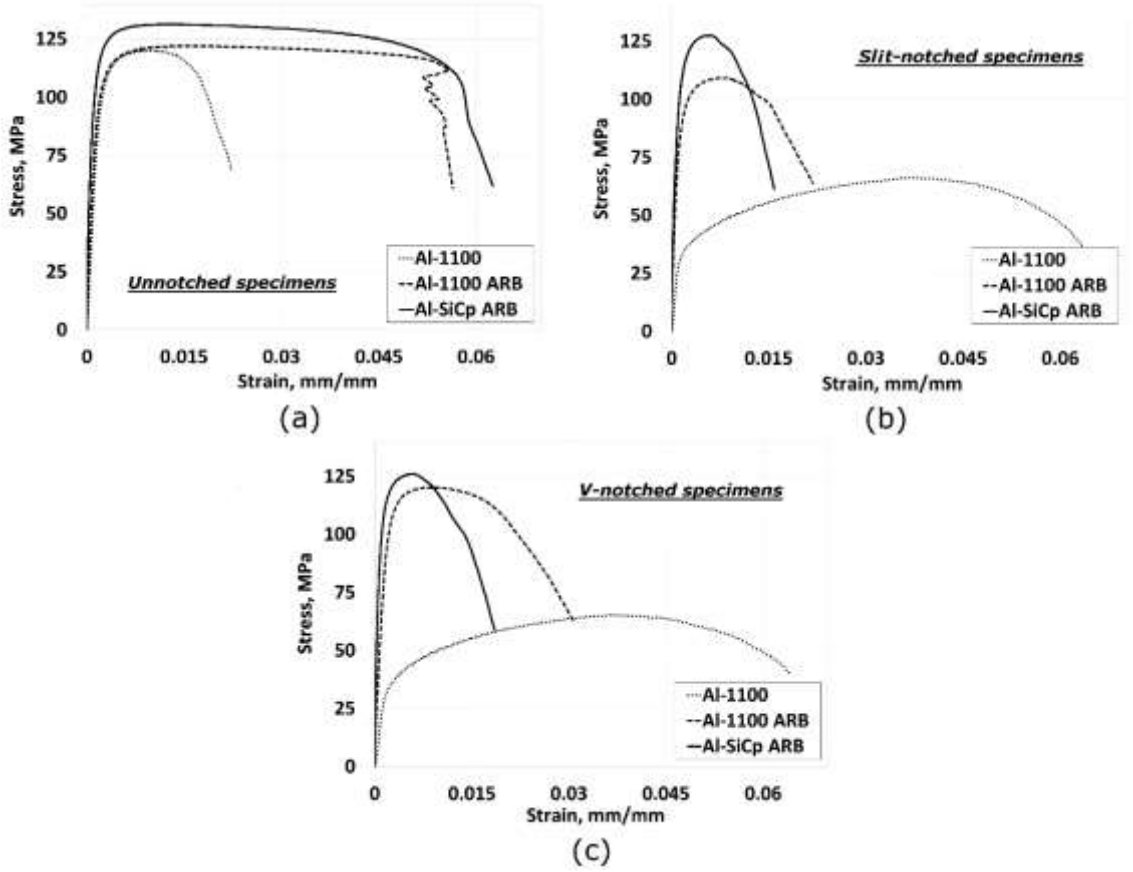

Figure 12. Engineering stress-strain curves for the three specimen geometries according to the material tested.

Figure 13 portrays the tensile fracture surfaces created in the materials tested in different specimen geometries.

Figures 13(a-c), corresponding to the Al-1100 sheet, reveals ductile fracture typical of aluminum and its alloys, with microcavities nucleation, growth and coalescence occurring in the mid-thickness of all specimen geometries [15,22,24], where plane-strain condition prevails. Conversely, regions next to the specimen surface deform by pure shear (plain-

stress condition). Notched specimens (Figs.13b,c) present a pronounced striation-like shear pattern (top and bottom of images) indicating that stress concentrators favor plastic deformation, thus confirming results provided in Fig11(a).

The fully ductile fracture of Al-1100 ARB laminate in the unnotched condition is observed in Fig.13(d), thus complying with respective stress-strain curve in Fig.11(b). On the other hand, notched specimens (Figs.13e,f) display somewhat brittle fracture aspects in the form of delaminations. The slit-notched specimen exhibits higher concentration of delamination sites than the V-notched one, though the latter condition depicts longer delaminations. Since stress-strain curves in Fig.11(b) indicate the slit-notch as the most severe condition in terms of mechanical performance, potential delamination sites should then be avoided in this material, e.g., by minimizing SiCp clusters.

Fully ductile fracture is also noticed in Fig.13(g) for unnotched MMC specimen, which agrees with stress-strain data in Fig.11(c). Figures 13(h,i) do not reveal any marked difference in fracture aspect of slit and V-notched specimens, which agrees with the almost identical behavior exhibited by the composite laminate when notched in one and other condition.

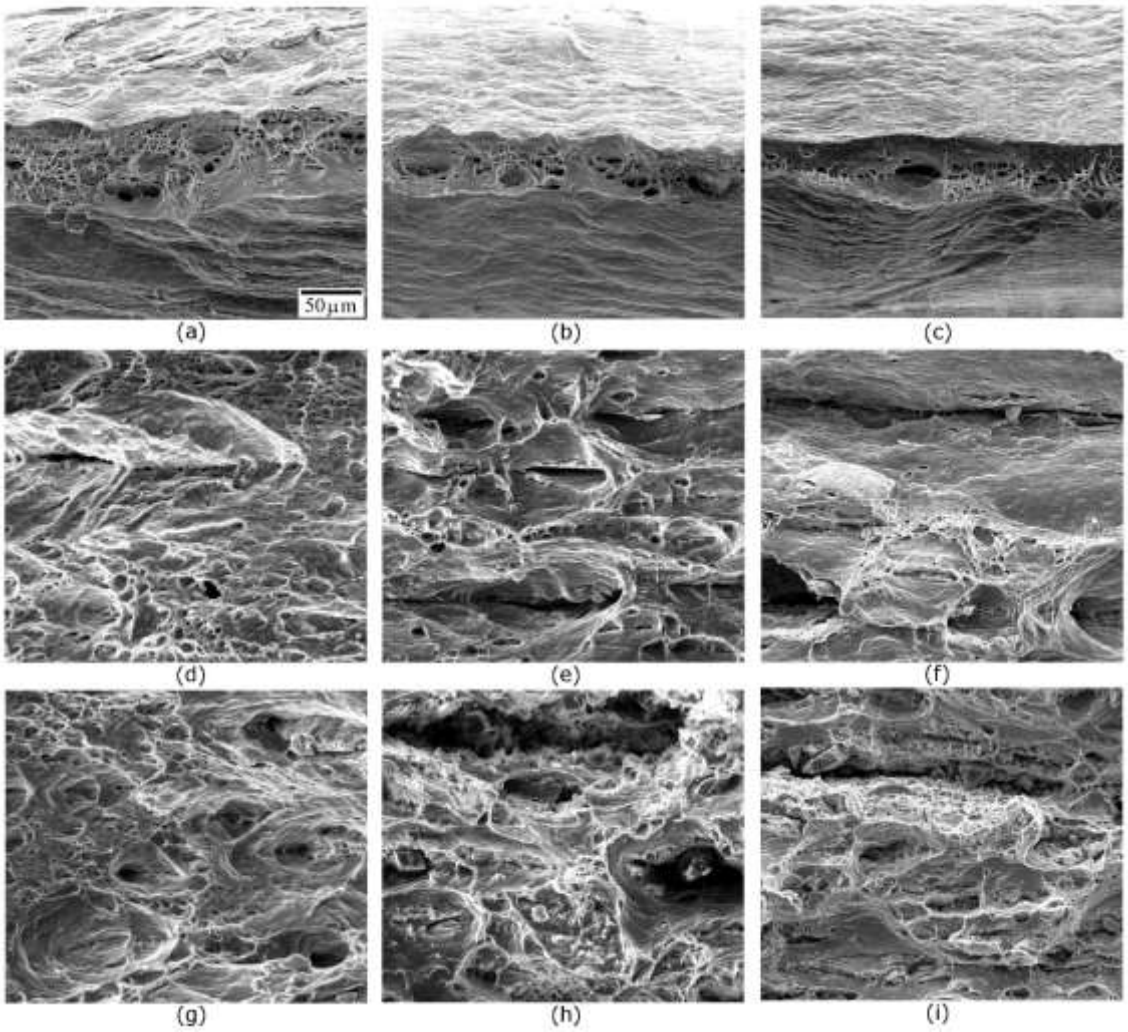

Figure 13. SEM images (SE mode) of tensile fracture surfaces: (a-c) as-received Al-1100 in unnotched, slit-notched and V-notched conditions, respectively; (d-f) the same sequence for Al-1100 ARB laminate; (g-i) the same for SiCp-A1100 MMC ARB laminate. Rolling direction and laminate thickness are parallel to, respectively, the page width and height. Images taken at same magnification.

Despite the best overall tensile performance presented by the ARB-MMC laminate, it did not catch up with similar materials reported in the literature [2,4,5,12-24,26-28,36,37,44,45], though it approached well some reported results related to warm-laminated ARB composites [15,22]. In this regard, limited grain refinement and scarcely accumulated strain-hardening, restricted SiCp agglomeration breakage and so particulate dispersion, besides porosity-reduced effective cross-section area [5,16,24] may have undermined the tensile behavior of the MMC laminate.

4.2.3 Wear testing

Table 5 shows the mean diameter values of the worn calottes in the Al-1100 and Al-SiCp MMC ARB laminates, as obtained by optical microscopy (OM) measurements for different wear test stages.

Table. Wear testing results for the ARB laminates.

Time (min)	Calotte diameter Al-1100 ARB		Calotte diameter Al-SiC_p MMC ARB		Travelled distance (m)
	Mean (mm)	SD	Mean (mm)	SD	
5	1.77	0.04	0.67	0.13	120
10	2.08	0.01	0.77	0.02	239
20	2.46	0.02	0.80	0.17	478
40	2.95	0.08	1.02	0.15	957

Figure 14 shows wear resistance curves, where it is evident the successful incorporation SiC particles by increasing the wear performance (volumetric loss criterion) of the Al-1100 ARB laminate by almost two orders of magnitude. This result is quite significant, even though there is no data available in the literature regarding similar wear test performed in Al-SiCp ARB laminates. In fact, the only one wear test result refers to pin-on-flat experiments carried out by Darmiani et al. [23], who reported mass loss reduction by half due to SiCp incorporation at 2 wt%.

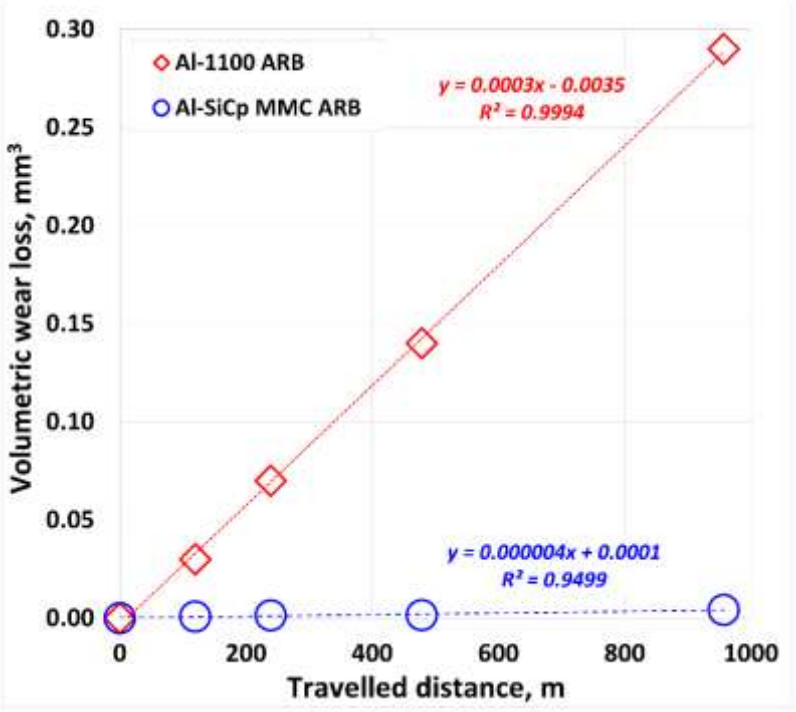

Figure 14. Wear resistance curves for the ARB laminates.

Figure 15(a) portrays OM views of worn surfaces of the materials tested. From left to right, one can see spherical calottes formed at test times of, respectively, 5 min, 10 min, 20 min and 40 min. From top to bottom, as-received Al-1100 strip, Al-1100 ARB and Al-SiCp MMC ARB laminates are displayed.

For both laminated materials, three predominant wear mechanisms can be identified, namely, abrasion and adhesion producing dark grooving marks, and delamination presenting bright alveolar aspect. In delamination, the material is worn in a layer-by-layer basis, while the material loss by abrasion and adhesion occurs by friction mechanism, which is intensified by delamination.

SEM views of worn surfaces of ARB materials are presented for two test times (respectively, 5 and 40 min) in Figs.15(b,c) for pure Al-1100, and Figs.15(b,c) for Al+SiCp laminates. Significantly more widespread wear damages are noticed in the former laminate. Also, large flat areas presenting gleamy aspect can be observed in the later laminate, giving signs that a surface layering material was formed during the repeated contact events. Recalling the earlier described tensile behavior of the MMC ARB laminate, and the proposed microstructural aspects leading to its somewhat poor performance (Subitem 4.2.2), it can be also postulated that its exceptional wear properties

are mainly due to the solid lubricant action of the ceramic particulate reinforcing phase. This effect substantially reduces the temperature at the contacts between the worn surface and the test ball, and so the friction coefficient of the system [16].

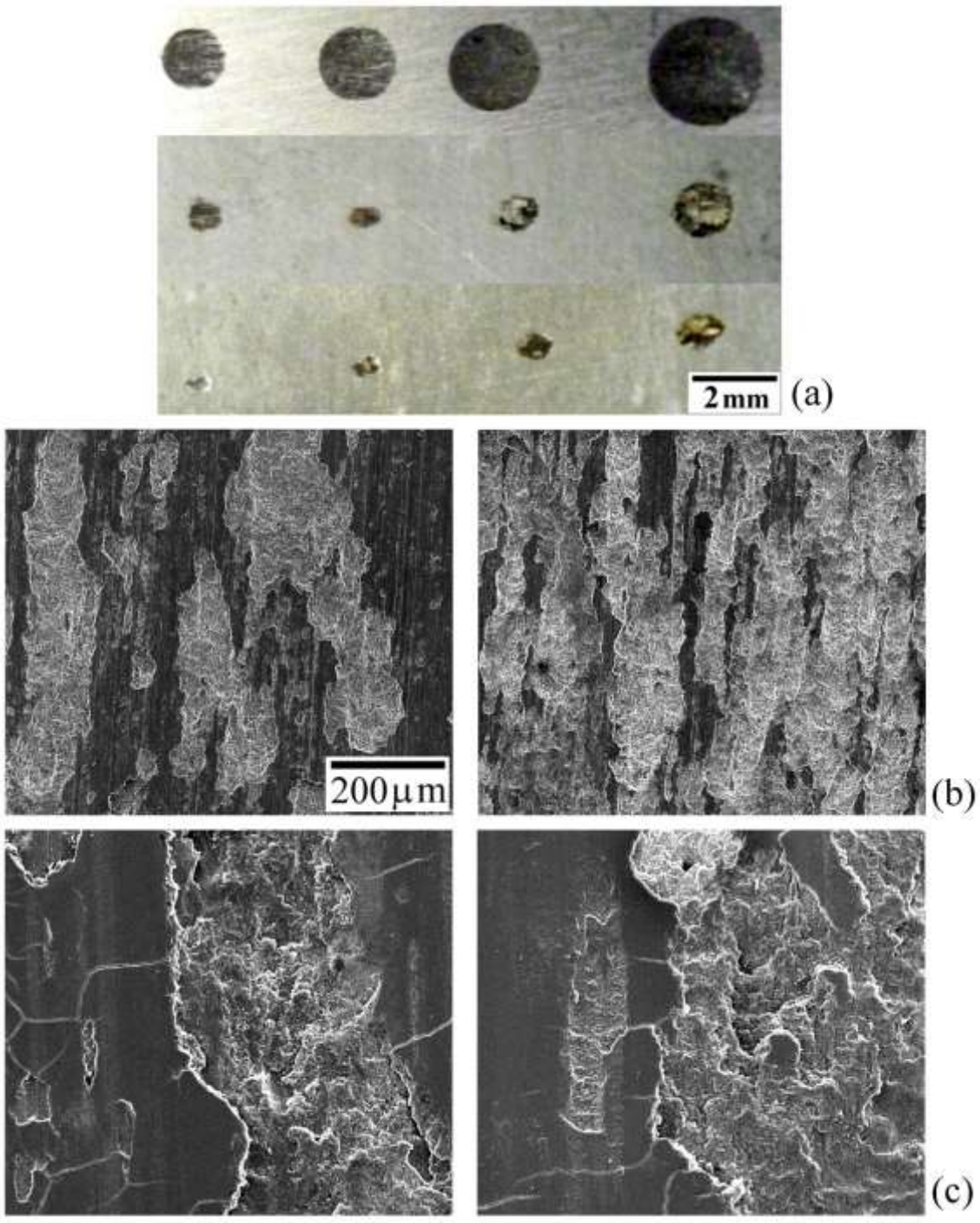

Figure 15. (a) OM fractographic views of four different wear test times: respectively, at 5, 10, 20 and 40 min. (b,c) SEM fractographic views (SE mode) of ARB Al-1100, and

(d,e) Al-SiCp ARB samples: (a,b) 5 min and (c,d) 40 min Al-1100 ARB, (e,f) 5 min and (g,h) 40 min Al-SiCp ARB.

5. Conclusions

Micro-silicon carbide particles (SiCp at 5 wt%) was incorporated to commercially pure aluminum 1100 by affordable accumulative roll bonding route. Microstructural changes and their effect on the mechanical properties and fracture mechanisms have been studied. Main conclusions are as follows:

i. Seven lamination passes reasonably dispersed SiCp in the aluminum matrix.
ii. SiC imparted hardness and only moderately enhanced tensile properties of unnotched and notched specimens.
iii. Tensile properties of the metal matrix laminate were insensitive to geometrical stress raisers.
iv. SiCp granted outstanding wear resistance to the composite laminate by acting as efficient solid lubricant.
v. Ductile fracture mechanisms prevailed in tensile loading, while abrasion, adhesive and lamination mechanisms governed wear properties.

Acknowledgments: One of the authors (Pereira G.S.) acknowledges the National Council for Scientific and Technological Development (CNPq-Brazil) for scholarship (Process: 160283/2014-0). This study was partly financed by Coordination for Improvement of Higher Education Staff (CAPES-Brazil) through Financial Support Code 001.

References

[1] Liu, Q.; Qi, F.; Wang, Q.; Ding, H.; Chu, K.; Liu, Y.; Li, C. The influence of particles size and its distribution on the degree of stress concentration in particulate reinforced metal matrix composites. *Materials Science & Engineering A*, **2018**,

v.731,p.351-359. https://doi:10.1016/j.msea.2018.06.067

[2] Khadir, A.I.; Fathy, A. Enhanced strength and ductility of Al-SiC nanocomposites synthesized by accumulative roll. *Journal of Materials Research and Technology*, **2019**, v.9, p.478-489. https://doi.org/10.1016/j.jmrt.2019.10.077

[3] Garg, P.; Jamwal, A.; Kumar, D.; Sadasivuni K.K.; Hussain, C.M.; Gupta, P. Advance research progresses in aluminium matrix composites: manufacturing & applications. *Journal of Materials Research and Technology*, **2019**, v.9, p.4924-4939. https://doi.org/10.1016/j.jmrt.2019.06.028

[4] Alizadeh, M.; Paydar, M.H. Fabrication of nanostructure Al/SiCP composite by accumulative roll-bonding (ARB) process. *Journal of Alloys and Compounds*, **2010**, v.492, p. 231-235. https://doi.org/10.1016/j.jallcom.2009.12.026

[5] Alizadeh, M.; Paydar, M.H. Fabrication of Al/SiCP composite strips by repeated roll-bonding (RRB) process. *Journal of Alloys and Compounds*, **2009**, v.477, p.811-816. https://doi.org/10.1016/j.jallcom.2008.10.151

[6] Saito, Y.; Tsuji, N.; Utsunomiya, H.; Sakai, T.; Hong, R.G. Ultra-fine grained bulk aluminum produced by accumulative roll-bonding (ARB) process. *Scripta Materialia*, **1998**, v.39, p.1221-1227. https://doi.org/10.1016/S1359-6462(98)00302-9

[7] Saito, Y.; Utsunomiya, H.; Tsuji, N.; Sakai, T. Novel ultra-high straining process for bulk materials-development of the accumulative roll-bonding (ARB) process. *Acta Materialia*, **1999**, v.47, p.579-583. https://doi.org/10.1016/S1359-6454(98)00365-6

[8] Ruppert, M.; Bohm, W.; Nguyen, H.; Hoppel, H.W.; Merklein, M.; Goken, M. Influence of upscaling accumulative roll bonding on the homogeneity and mechanical properties of AA1050A. *Journal of Materials Science*, **2013**, v.48, p.8377-8385. https://doi.org/10.1007/s10853-013-7648-3

[9] Chen, M.; Hsieh, C.; Wu, W. Microstructural characterization of Al/Mg alloy interdiffusion mechanism during accumulative roll bonding. *Metals and Materials International*, **2007**, v.13, p.201-205. https://doi.org/10.1007/BF03027805

[10] Li, B.L.; Tsuji, N.; Kamikawa, N. Microstructure homogeneity in various metallic materials heavily deformed by accumulative roll-bonding. *Materials Science and Engineering: A*, **2006**, v.423, p.331-342. https://doi.org/10.1016/j.msea.2006.02.028

[11] Tsuji, N.; Saito, Y.; Lee, S.; Minamino, Y. ARB (accumulative roll-bonding) and other new techniques to produce bulk ultrafine grained materials. *Advanced Engineering*

Materials, **2003**, v.5, p.338-344. https://doi.org/10.1002/adem.200310077

[12] Jamaati, R.; Toroghinejad, M.R. Investigation of the parameters of the cold roll bonding (CRB) process. *Materials Science and Engineering: A*, **2010**, v.527, p.2320-2326. https://doi.org/10.1016/j.msea.2009.11.069

[13] Amirkhanlou, S.; Rahimian, M.; Ketabchi, M.; Parvin, N.; Yaghinali, P.; Carreño, F. Strengthening mechanisms in nanostructured Al/SiCp composite manufactured by accumulative press bonding. *Metallurgical and Materials Transactions A*, **2016**, v.47, p.5136-5145. https://doi.org/10.1007/s11661-016-3666-5

[14] Liu, C.Y.; Wang, Q.; Jia, Y.Z.; Zhang, B.; Jing, R.; Ma, M.Z.; Jing, Q.; Liu, R.P. Evaluation of mechanical properties of 1060-Al reinforced with WC particles via warm accumulative roll bonding process. *Materials & Design*, **2013**, v.43, p.367-372. https://doi.org/10.1016/j.matdes.2012.07.019

[15] Farhadipour, P.; Sedighi, M.; Vini, M.H. Using warm accumulative roll bonding method to produce Al-Al2O3 metal matrix composite. *Proceedings of the Institution of Mechanical Engineers, Part B: Journal of Engineering Manufacture*. **2017**, v.231, p.889-896. https://doi.org/10.1177/0954405417703421

[16] Ghalehbandi, S.M.; Malaki, M.; Gupta, M. Accumulative roll bonding - a review. *Applied Sciences*, **2019**, v.9, p.3627-3659. https://doi.org/10.3390/app9173627

[17] Lee, S.H.; Kim, W.J.; Utsunomiya, H. Fabrication and evaluation of nanostructure Al-SiCp composite by accumulative roll-bonding. *Journal of Nanoscience and Nanotechnology*, **2011**, v.11, p.7451-7455. https://doi.org/10.1166/jnn.2011.4767

[18] Alizadeh, M.; Paydar, M.H.; Terada, D., Tsuji, N. Effect of SiC particles on the microstructure evolution and mechanical properties of aluminum during ARB process. *Materials Science and Engineering: A*, **2012**, v.540, p.13-23. https://doi.org/10.1016/j.msea.2011.12.026

[19] Jamaati, R.; Amirkhanlou, S.; Toroghinejad, M.R.; Niroumand, B. Effect of particle size on microstructure and mechanical properties of composites produced by ARB process. *Materials Science and Engineering: A*, **2012**, v.528, p.2143-2148. https://doi.org/10.1016/j.msea.2010.11.056

[20] Wagih, A.; Fathy, A.; Ibrahim, D.; Elkady, O.; Hassan, M. Experimental investigation on strengthening mechanisms in Al-SiC nanocomposites and 3D FE simulation of Vickers indentation. *Journal of Alloys and Compounds*, **2018**, v.752, p.137-

147. https://doi.org/10.1016/j.jallcom.2018.04.167

[21] Melaibari, A.; Fathy, A.; Mansouri, M.; Eltaher, M.A. Experimental and numerical investigation on strengthening mechanisms of nanostructured Al-SiC composites. *Journal of Alloys and Compounds*, **2019**, v.774, p.1123-1132. https://doi.org/10.1016/j.jallcom.2018.10.007

[22] Fathy, A.; Ibrahim, D.; Elkady, O. Hassan, M. Evaluation of mechanical properties of 1050-Al reinforced with SiC particles via accumulative roll bonding process. *Journal of Composite Materials*, **2019**, v.53, p.209-218. https://doi.org/10.1177/0021998318781462

[23] Darmiani E.; Danaee I.; Golozar M.A.; Toroghinejad M.R.; Ashrafi A.; Ahmadi A. Reciprocating wear resistance of Al-SiC nano-composite fabricated by accumulative roll bonding process. *Materials & Design*, **2013**, v.50, p.497-502. https://doi.org/10.1016/j.matdes.2013.03.047

[24] Amirkhanlou S.; Jamaati R.; Niroumand B.; Toroghinejad M.R. Fabrication and characterization of Al/SiCp composites by CAR process. *Materials Science and Engineering A,* **2011**, v.528, p.4462-4467. https://doi.org/10.1016/j.msea.2011.02.037

[25] Gee, M.; Gant, A.J.; Hutchings, I.M.; Kusano, Y.; Schiffman, K.; Van Acker, K.; Poulat, S.; Plint, G. Results from an interlaboratory exercise to validate the micro-scale abrasion test. *Wear*, **2005**, v.259, p.27-35. https://doi.org/10.1016/j.wear.2005.02.092

[26] Santos Filho, O.C. Microestrutural and mechanical properties characterization of AA1100 and AA5052 alloys processed by accumulated roll bonding - ARB. Master's Dissertation. Politechnic School of Metallurgy and Materials Engineering. http://dx.doi.org/10.11606/D.3.2009.tde-29062009-103030

[27] Kaneko, S.; Fukuda, K.; Utsunomiya, H.; Sakai, T.; Saito, Y.; Furushiro, N. Ultra Grain refinement of aluminium 1100 by ARB with cross rolling. *Materials Science Forum*, **2003**, v.426, p.2649-2654. https://doi.org/10.4028/www.scientific.net/MSF.426-432.2649

[28] Kwan, C.; Wang, Z.; Kang, S.B. Mechanical behavior and microstructural evolution upon annealing of the accumulative roll-bonding (ARB) processed Al alloy 1100. *Materials Science and Engineering: A*, **2008**, v.480, p.148-159. https://doi.org/10.1016/j.msea.2007.07.022

[29] Bagherpour, E.; Reihanian, M.; Miyamoto, H. Tailoring particle distribution Non-

uniformity and grain refinement in nanostructured metal matrix composites fabricated by severe plastic deformation (SPD): a correlation with flow stress. *Journal of Materials Science*, **2017**, v.52, p.3436–3446. https://doi.org/10.1007/s10853-016-0632-y

[30] Khadir, A.I.; Fathy, A. Enhanced strength and ductility of Al-SiC nanocomposites Synthesized by accumulative roll bonding. *Journal of Materials Research and Technology*, **2019**, 12p. https://doi.org/10.1016/j.jmrt.2019.10.077

[31] Meselhy, A.F.; Reda, M.M. Investigation of mechanical properties of nanostructured Al-SiC composite manufactured by accumulative roll bonding. *Journal of Composite Materials*, **2019**, v.53, p.3951–3961. https://doi.org/10.1177/0021998319851831

[32] Oliveira, J.D.C.P.T.; Padilha, A.F. Microstructural characterization of AA1100, AA1050 and AA1070 commercial aluminums and AA1199 super pure aluminum. *Rem: Revista Escola de Minas*, **2009**, v.62, p.373-378. http://dx.doi.org/10.1590/S0370-44672009000300017.

[33] Adam, K.; Zöllner, D.; Field, D.P. 3D microstructural evolution of primary recrystallization and grain growth in cold rolled single-phase aluminum alloy. *Modelling and Simulation in Materials Science and Engineering*, **2018**, v.26, 16p. https://doi.org/10.1088/1361-651X/aaa146

[34] Kondo, S.; Mitsuma, T.; Shibata, N.; Ikuhara, Y. Direct observation of individual dislocation interaction processes with grain boundaries. *Science Advances*, **2016**, v.2, 11p. https://doi.org/10.1126/sciadv.1501926

[35] Shamanian, M.; Mohammadnezhad, M.; Asgari, H.; Szpunar, J. Fabrication and characterization of Al-Al2O3-ZrC composite produced by accumulative roll bonding (ARB) process, *Journal of Alloys and Compounds*, **2015**, v.618, p.19-26. https://doi.org/10.1016/j.jallcom.2014.08.136

[36] Heydari V.M.; Farhadipour, P. Fabrication of AA1060/Al2O3 composites by warm accumulative roll bonding process and investigation of its mechanical properties and microstructural evolution. *International Journal of Advanced Design and Manufacturing Technology*, **2017**, v.10, p.91-98. https://www.magiran.com/paper/1781372

[37] Yousefian, R.; Emadoddin, E.; Baharnezhad, S. Manufacturing of the aluminum metal-matrix composite reinforced with micro-and nanoparticles of TIO2 through

accumulative roll bonding process (ARB). *Reviews on Advanced Materials Science*, **2018**, v.55; p.1-11. https://doi.org/10.1515/rams-2018-0022

[38] Cepeda-Jiménez, C., Pozuelo, M., García-Infanta, J. Interface effects on the fracture mechanism of a high-toughness aluminum-composite laminate. *Metallurgical and Materials Transactions A*, **2009,** v.40 p.69-79. https://doi.org/10.1007/s11661-008-9679-y

[39] Chen, Z.; Chen, Q. Interface shear actions and mechanical properties of nanostructured dissimilar al alloy laminated metal composites. *Journal of Nanomaterials*, **2015**, v.2015, 14p. http://dx.doi.org/10.1155/2015/612029

[40] Huang, C.X.; Wang, Y.F.; Ma, X.L.; Yin, S.; Höppel, H.W.; Göken, M.; Wu, X.L.; Gao, H.J.; Zhu, Y.T. Interface affected zone for optimal strength and ductility in heterogeneous laminate. *Materials Today*, **2018**, v.21, p.713-719. https://doi.org/10.1016/j.mattod.2018.03.006

[41] Sobie, C.; McPhie, M.G.; Capolungo, L.; Cherkaoui, M. The effect of interfaces on the mechanical behaviour of multilayered metallic laminates. *Modelling and simulation in materials science and engineer*ing, **2014**, v.22, 14p. https://doi.org/10.1088/0965-0393/22/4/045007

[42] Qu, R.; Zhang, P.; Zhang, Z. Notch effect of materials: strengthening or weakening? *Journal of Materials Science & Technology*, **2014**, v.30, p.599-608. https://doi.org/10.1016/j.jmst.2014.04.014

[43] Shin, S.; Cho, S.; Lee, D.; Kim, Y.; Lee, S.B.; Lee, S.K.; Jo, I. Microstructural evolution and strengthening mechanism of SiC/Al composites fabricated by a liquid-pressing process and heat treatment. *Materials*, **2019**, v.12, p.3374-3384. https://doi.org/10.3390/ma12203374

[44] Min, S.O.N.G. Effects of volume fraction of SiC particles on mechanical properties of SiC/Al composites. *Transactions of Nonferrous Metals Society of China*, **2009**, v.19, 1400-1404. https://doi.org/10.1016/S1003-6326(09)60040-6

[45] Liu, C.Y.; Jiang, H.J.; Wang, C.X.; Li, Y.P.; Luo, K. Fabrication and strengthening mechanisms of Al/WC particles composite prepared by accumulative roll bonding. *Materials Science Forum*, **2016,** v.849, p.397-401. https://doi.org/10.4028/www.scientific.net/msf.849.397